Fluorescence characteristics of the fuel tracer 1-methylnaphthalene for the investigation of equivalence ratio and temperature in an oxygen-containing environment

Ulrich Retzer[1,2] · Wolfgang Fink[1] · Thomas Will[1] · Stefan Will[1,2] · Lars Zigan[1,2]

Abstract

In this work, the fluorescence properties of the fuel tracer 1-methylnaphthalene (1-MN) are investigated in a calibration flow cell at elevated temperatures and pressures. This fuel tracer is well suited to investigate mixture formation in diesel engine applications, as 1-MN is a natural diesel fuel component. A tracer-LIF (laser-induced fluorescence) concept is developed that enables temperature measurements using a two-color approach in oxygen-containing gas mixtures. Furthermore, the potential for simultaneous measurement of equivalence ratio (fuel–air ratio, FAR) is evaluated. First, a picosecond Nd:YLF-laser at 263 nm in combination with a spectrograph and a streak unit was used to investigate the spectral fluorescence emission and fluorescence lifetimes. In addition, a nanosecond Nd:YAG-laser at 266 nm was used for fluorescence calibration with regard to equivalence ratio and temperature. All measurements were performed in an oxygen-containing environment at different equivalence ratios, temperatures up to 800 K and pressures up to 2.5 MPa. The dependency of the fluorescence emission on equivalence ratio was studied for varied fuel amount and air concentrations. The calibration data form the basis for investigations of fuel distribution and temperature under realistic engine conditions in an oxygen-containing environment.

1 Introduction

It is necessary to optimize the mixing process of fuel and air in an internal combustion (IC) engine to achieve a high efficiency and low pollutant emissions. For this purpose, the temperature distribution and the local fuel/air mixture composition, often described in the form of equivalence ratio, must be determined.

A suitable measurement technique to determine these parameters is planar laser-induced fluorescence (PLIF). This technique is based on photon absorption by molecules

✉ Lars Zigan
  lars.zigan@fau.de

  Ulrich Retzer
  ulrich.retzer@fau.de

1 Lehrstuhl für Technische Thermodynamik (LTT), Universität Erlangen-Nürnberg, Erlangen, Germany

2 Erlangen Graduate School in Advanced Optical Technologies (SAOT), Universität Erlangen-Nürnberg, Erlangen, Germany

(mostly in the UV range) and subsequent emission of red-shifted fluorescence. Typically tracer substances, added to the fuel and/or air, with appropriate fluorescence characteristics are used. The fluorescence signal can be affected by temperature, pressure, mixture composition (or equivalence ratio) and excitation wavelength. For quantitative investigations of the mixture formation, it is necessary to know all these interrelations on the LIF signal. Therefore, before applying these tracers to a technical system, the exact fluorescence behavior of these tracers has to be investigated and calibrated at defined temperature, pressure and mixture composition.

For mixing studies, the tracer substances are typically seeded to a non-fluorescent substitute fuel. It is essential that the physical and chemical properties of fuel and fluorescence tracer are comparable for a precise description of the involved processes. Especially, a similar evaporation behavior of fuel and tracer is important for the quantification of the equivalence ratio and the temperature, which limits the selection of suitable diesel fuel tracers [1].

Typical LIF tracers belong to the groups of ketones [2, 3], aromatics [4–6] or amines [7, 8]. Acetone [9] and 3-pentanone [10] fluorescence shows a direct dependency on the tracer mole fraction so that a measurement of the fuel

concentration is possible. For this purpose, the local temperature must be known, which—when using these ketones—can favorably be determined by two-line excitation LIF [2, 10]. This approach requires two laser wavelengths, and typically the lines 248 nm and 308 nm emitted by excimer lasers are utilized [10–12].

In contrast to most ketones, the fluorescence of aromatics and amines is usually quenched by oxygen, which is part of the surrounding atmosphere. This fluorescence quenching depends on the local oxygen concentration and it can thus be used for determining the equivalence ratio/fuel-air-ratio (FAR-LIF) [13]. There are many FAR-LIF tracer concepts that were mainly developed for spark-ignition (SI) engines. Triethylamine (TEA) upon excitation at 248 nm [8, 14–19] and 266 nm [20, 21] was already used to investigate the FAR in gasoline engines. These studies indicated a linear dependency of the fluorescence intensity on the FAR. This tracer only shows a weak temperature dependency of the LIF signals for temperatures up to 350 °C [22]. Furthermore, biacetyl was used for quantitative measurements of FAR in gasoline engines [23, 24] upon excitation at 355 nm. However, less calibration data exist for this fuel tracer, and the signal is relatively weak under technically relevant conditions [9].

Toluene is a well-characterized FAR-LIF tracer, which is also used for investigating of the mixture formation at SI engine conditions. Toluene additionally shows a spectral red-shift with increasing temperature, which enables temperature determination by two-color-detection. In this technique, the emission spectrum is separated into a "blue" and a "red" channel. The temperature-dependent intensity ratio of these two channels has to be calibrated at known conditions [6, 25–28] and can then be used for temperature determination in technical applications [29–32]. Most temperature measurements in SI engines were performed in pure nitrogen atmosphere, as the signal ratio is strongly dependent on the oxygen partial pressure [26]. Typically, aromatic LIF tracers show a spectral red-shift and broadening and, therefore, are adopted for two-color-thermometry. Examples are anisole, which was used as LIF tracer to investigate the FAR and temperature during mixture formation under SI engine conditions [33, 34], and *p*-xylene [35].

Naphthalene [25, 36, 37], 1-methylnaphthalene (1-MN) [4, 36] and 2-methylnaphthalene as well as 1-phenyloctane and 1-phenyldecane [4] are suitable tracers for diesel engine applications as they match the substance properties of diesel fuel very well. It has been shown that 1-MN is the most promising tracer as it can be seeded easily to liquid diesel-like fuels and the signal intensity in nitrogen is very high even at elevated temperatures [4]. 1-MN has a relatively high absorption cross-section of 1.28×10^{-17} cm^2 (at 266 nm and 350 K) [37]. In comparison, the absorption cross-section of toluene at 350 K and 266 nm is about 2.6×10^{-19} cm^2

[6]. Furthermore, the fluorescence quantum yield of 1-MN is typically three orders of magnitude larger than that of ketones and larger than the quantum yield of toluene [37]. For example, at 298 K and 0.1 MPa 1-MN (liquid solution in cyclohexane) has a fluorescence quantum yield of 0.25 [38], whereas the quantum yield of pure toluene is about 0.19 [39].

1-MN has already been used for qualitative fuel distribution measurements [40] and quantitative temperature and fuel distribution measurements [5] in a diesel spray. Furthermore, it was applied for mixing studies in a transparent diesel engine to study effects of swirl and pilot injection mass on fuel distribution. However, these measurements were carried out in nitrogen atmosphere. First calibration measurements in air were performed at ambient pressure conditions in heated free jets [36]. In this work, a linear dependency of 1-MN fluorescence on the equivalence ratio was shown. However, this was accompanied by a strong nonlinear temperature dependency. Furthermore, as the quenching effect is a collisional process, also elevated pressures must be investigated. In this work, the FAR-LIF concept using 1-MN is evaluated at temperatures up to 798 K and at pressures up to 2.5 MPa. Furthermore, the two-color concept is investigated in a wide range of pressures, temperatures and equivalence ratios.

2 Theoretical background

The fluorescence signal of a special tracer molecule depends on absorption processes and non-radiative transitions competing with fluorescence, such as vibrational relaxation, intersystem crossing, internal conversion and quenching. If the fluorescence intensity of a tracer is in the linear regime (i.e., if the signal is proportional to the laser energy) while pressure, temperature and excitation wavelength are known and constant at a specific operation condition, the fluorescence signal can be described as:

$$S_\mathrm{fl} \sim \sigma_\mathrm{abs}(T, \lambda_\mathrm{ex}) \cdot n_\mathrm{fl} \cdot \Phi_\mathrm{fl}(T, p, \lambda_\mathrm{ex}, \chi_\mathrm{i}), \qquad (1)$$

with

$$\Phi_\mathrm{fl} = \frac{k_\mathrm{fl}}{k_\mathrm{fl} + k_\mathrm{nr} + \tilde{k}_\mathrm{q} \cdot n_\mathrm{q}}. \qquad (2)$$

Here, σ_abs is the absorption cross-section, which depends on temperature T and excitation wavelength λ_ex; Φ_fl is the fluorescence quantum yield, which depends on the temperature T, pressure p, excitation wavelength λ_ex and gas composition χ_i. The terms n_fl and n_q are the number densities of fluorescent tracer molecules and the quenching molecules, respectively. k_i describes the rate of the respective process

separated according to fluorescence (k_{fl}), non-radiative processes (k_{nr}) and the quenching process, which is defined by the rate coefficient ($\tilde{k}_q$) multiplied by the number density of quenching molecules n_q.

2.1 FAR-LIF

If the quenching process is very fast in comparison to the other non-radiative transitions, the signal intensity becomes directly proportional to the ratio of fluorescent tracer molecules and quenching molecules. If the tracer represents the fuel while oxygen is the only relevant quenching molecule, the signal intensity becomes directly proportional to the equivalence ratio Φ. Under this so-called "FAR-LIF assumption", the fluorescence signal intensity S_{fl} can then be described as [1]:

$$S_{fl} \sim \frac{n_{fl}}{n_q} \sim \frac{n_{tracer/fuel}}{n_{oxygen}} \sim \Phi. \tag{3}$$

As mentioned above, this assumption is valid if the fluorescence signal does not depend on temperature and pressure or if these two quantities are known (measured) so that the signal intensity is corrected accordingly. Usually, the quenching effect occurs if an excited, quenching-sensitive molecule collides with an oxygen molecule. During this energy transfer process, the oxygen molecule is electronically excited from its ground state (triplet) to its excited singlet state. However, this can only happen if the singlet–triplet energy difference of the tracer molecule is larger than the required energy to excite the oxygen molecule (91 kJ/mol) [1]. This is true for aromatics, which exhibit large triplet-singlet energy differences of about 120 kJ/mol (toluene).

2.2 Two-color-detection

Aromatic compounds usually show a temperature-dependent red-shift/broadening of the fluorescence emission spectrum, which can be used for temperature determination using a "two-color-detection" scheme as already mentioned in the introduction. An increased temperature results in a higher probability of reaching increased vibrational levels within the excited state S_1. Fluorescence emission from highly excited vibrational levels of S_1 leads to population of highly excited vibrational level of S_0 (increased excess energy). This results in a decreased fluorescence photon energy compared to an excitation process at lower energy (i.e., lower temperature), which explains the spectral red-shift of the fluorescence emission spectrum. This means that the red-shift of the emission is a function of the excess energy and this shift will be larger for molecules showing larger differences of the shapes and anharmonicities of the S_1 and S_0

potential energy curves [41]. Two-color-detection is based on simultaneous detection of two separate spectral ranges (λ_1 and λ_2) of such a temperature-dependent emission spectrum. The ratio of these two signal intensities can be mathematically described by [26]:

$$
\begin{aligned}
S_{ratio} = \frac{S_{\lambda 1}}{S_{\lambda 2}} &= \frac{\left[\eta_1 \cdot E \cdot n_{tracer} \cdot \sigma_{abs}(\lambda_{ex}, T) \cdot \Phi_{fl}(\lambda_{ex}, T, p, \chi_i)\right]_{\lambda 1}}{\left[\eta_2 \cdot E \cdot n_{tracer} \cdot \sigma_{abs}(\lambda_{ex}, T) \cdot \Phi_{fl}(\lambda_{ex}, T, p, \chi_i)\right]_{\lambda 2}} \\
&= \frac{\left[\Phi_{fl}(T)\right]_{\lambda 1}}{\left[\Phi_{fl}(T)\right]_{\lambda 2}}.
\end{aligned}
\tag{4}
$$

As only one excitation wavelength and one tracer substance are used, the laser fluence E, the tracer partial density n_{tracer} and the absorption cross-section σ_{abs} cancel out. The optical detection efficiency $\eta_{1/2}$ can be eliminated by a homogeneous reference image at known temperature. The temperature sensitivity of the ratio depends on the spectral filters used and may be a function of the oxygen partial pressure/equivalence ratio [26].

3 Experiment

In this experiment, imaging techniques are used to calibrate the fuel tracer 1-MN with respect to the equivalence ratio and to the temperature. In addition, spectral emissions and fluorescence decay times are characterized in a wide range of engine relevant conditions.

All measurements are performed in a continuously scavenged calibration flow cell (HTC^2), which can be operated up to 1000 K and 3.0 MPa. Temperature and pressure studied were in ranges of 400–800 K and 1–2 MPa, respectively, while the equivalence ratio Φ was varied from 0.67 to 2. In a typical passenger car, much higher pressures can be reached under full-load operation; however, the pressure effect on the LIF signal is small as discussed below. Lower temperatures and pressures (e.g., 400 K, 1 MPa) are less relevant for conventional diesel injection, but injection conditions similar to the conditions used on this work occur for very early pilot injections for partially premixed charged combustion concepts (PPCI) or homogenous charge compression ignition concepts (HCCI), see, e.g., Miles et al. [42]. In addition, the temperature information during compression can be determined using the presented tracer-LIF concept and the presented calibration data.

The calibration cell with supply system as well as both optical setups is shown in Fig. 1. The liquid fuel/tracer mixture is adjusted and vaporized by a controlled evaporating and mixing system (CEM, Bronkhorst). The gas flow is adjusted by mass flow controllers and heated up by heating cartridges. After the heating section, the fuel/tracer vapor and the gas flow are combined in a mixing section before
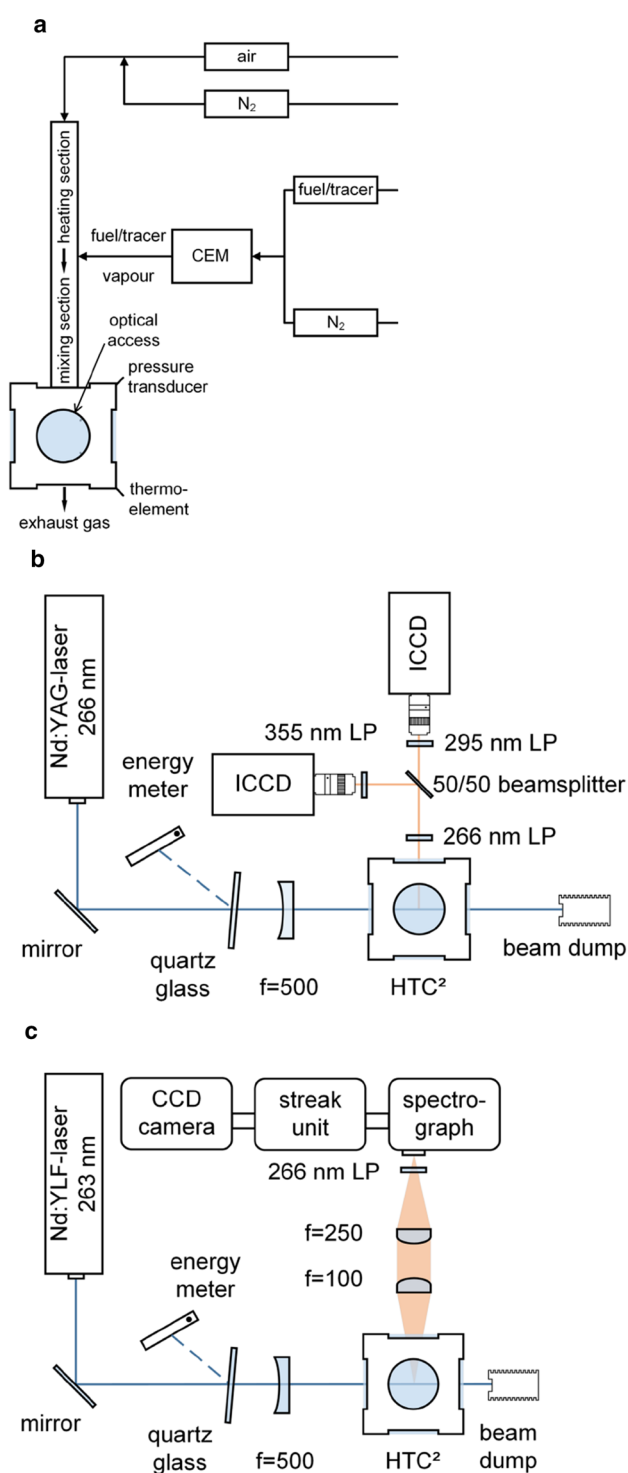
Fig. 1 **a** Sketch of the calibration cell HTC^2 and gas supply system, **b** optical setup for FAR-LIF and two-color-detection calibration, and **c** optical setup for spectral and temporal calibration

the heating elements. In addition, tracer reaction is reduced by a relatively short tracer residence time below 1 s inside the cell. The temperature in the measurement volume is determined by a thermocouple, which is mounted at the bottom of the cell. The spatial temperature profile in the chamber was measured in separate experiments using thermocouples, and it is taken into account during all calibration measurements. The pressure is determined by a pressure transducer, and it is adjusted by a backpressure regulator downstream the chamber. More information about the HTC^2 cell can be found elsewhere [4].

The cell was operated with an air/nitrogen mixture instead of pure air. This measure allows for a reduction of the required amount of fuel/tracer mixture (which is limited by the evaporator due to the maximum boiling temperature of 473 K) even for high equivalence ratios. In contrast to previous calibration measurements in pure nitrogen [43], the tracer was seeded at an increased fraction of 1 vol% (instead of 0.5 vol%) to the non-fluorescent substitute fuel. This volume fraction enables sufficiently high signal intensities despite the oxygen-quenching effect. Measurements in air show a linear dependency of signal intensity on tracer volume fraction in the fuel between 0.5 and 1 vol% at the given laser pulse energies and equivalence ratio. Isooctane was used as substitute fuel. It is a typical single-component fuel for gasoline applications and less suitable for diesel fuels. However, it shows a very high thermal stability compared to diesel surrogate fuels, which is necessary for high-temperature calibrations. In Table 1, an overview of fluid properties is given at 0.1 MPa for tracers, diesel fuel and surrogate fuels. For an appropriate tracer selection, a good match of the boiling point and the enthalpy of vaporization between tracer and fuel is crucial. 1-MN matches the enthalpy of vaporization and the boiling range of diesel fuel quite well. The boiling point of toluene, which was used as diesel tracer in former experiments [44–46], is significantly lower than the boiling range of diesel. This could lead to preferential evaporation of toluene. In this case, the tracer fluorescence does not represent the carrier fuel anymore.

For excitation of 1-MN, a Nd:YAG-laser at 266 nm was used with 5-ns pulse duration at 10 Hz repetition rate and a pulse energy of about 6 mJ. Before entering the cell through one of the four quartz glass windows (clear width of $d = 26$ mm), the beam was formed to a light sheet (~ 8 mm × 0.8 mm). About 5% of the laser beam is reflected onto an energy meter using a quartz glass plate for corrections of shot-to-shot fluctuations of the laser energy.

The fluorescence signal was detected perpendicularly to the laser sheet by ICCD cameras. To cut off scattered laser light, a 266-nm longpass filter was positioned between the cell and the cameras/spectrograph. For every operating point, three measurements of 50 images each are performed. Out of these 50 images, a mean value within a region of

entering the cell (Fig. 1a). This arrangement guarantees a homogeneous mixture inside the cell and reduces possible thermal decomposition and oxidation of the tracer caused by

Table 1 Summary of physical properties of different fuels and tracers

Species	Molar mass (g/mol)	Density at 298 K (kg/m^3)	Kin. viscosity at 313 K (mm^2/s)	Boiling point (K)	Enthalpy of vapori-zation (kJ/kg)	Ignition temperature (K)
1-MN	142.2[a]	1043[a]	5.321[a]	517.8[a]	327.3[e]	758[c]
Diesel	–	820–845[b]	2–4.5[b]	433–653[b]	354.5[f]	503 (55 CN)[d]
Isooctane	114.2[a]	694.6[a]	2.670[a]	372.4[a]	302.1[e]	683[c]
N-Hexadecane	226.4[a]	773.0[a]	6.112[a]	560.0[a]	231.6[e]	488[c]
Toluene	92.14[a]	857.7[a]	0.5461[a]	383.8[a]	360.8[e]	808[c]

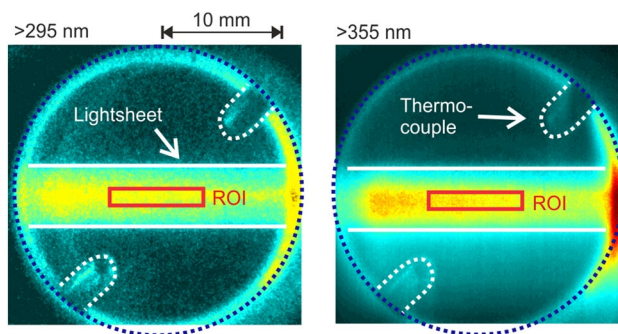*CN* cetane number

[a] [47]; [b] [48]; [c] [49]; [d] [50]; [e] [51]; [f] [52]

Fig. 2 Example of a single-shot fluorescence image of 1-MN at 598 K, 1.0 MPa and $\Phi = 1$ including ROI for value calculation

Fig. 3 Example of a temporally and spectrally resolved image of 1-MN fluorescence at 650 K in nitrogen atmosphere

interest (ROI) comprising 1750 pixels is calculated. All images were background corrected. The FAR-LIF measurements were performed using a PCO DiCam Pro 12 bit. The two-color-detection measurements were performed using an Andor iStar equipped with a Schott 295-nm longpass filter and a PCO DiCam Pro 12 bit equipped with a Semrock 355-nm longpass filter. These filters were selected for maximal signal intensity (SNR) and for high-temperature sensitivity (see the study in Trost et al. [4]). In this work, the two-color-detection and FAR-LIF calibration were performed in separate experiments but this could basically be done with a single setup. Figure 2 shows an example of a single-shot fluorescence image of 1-MN at 598 K, 1.0 MPa and $\Phi = 1$ including the ROI.

To obtain additional spectral and temporal information, a streak camera (C10910-01, Hamamatsu Photonics) equipped with a spectrograph (Acton SP2300, Princeton Instruments) was used (Fig. 1c). The spectrograph is operated with a 150 g/mm grating at a blaze wavelength of 300 nm. The LIF signal was collected by a spherical lens ($f = 100$ mm) and subsequently focused onto the slit of the spectrograph by a second spherical lens ($f = 250$ mm). After passing the spectrograph and the streak camera, the LIF signal is now temporally (*y*-axis) and spectrally (*x*-axis) resolved (see Fig. 3). This two-dimensional information was detected by a
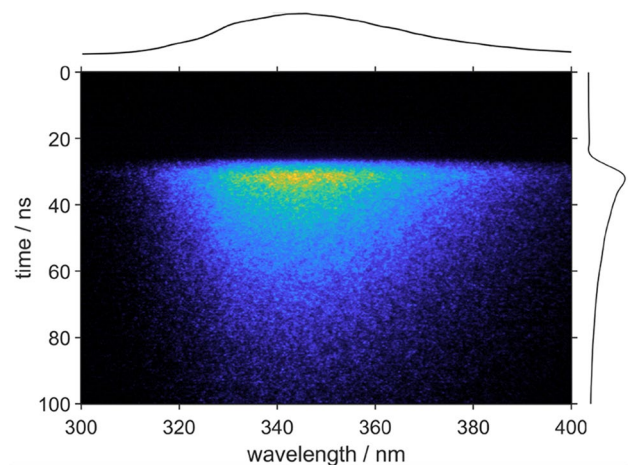
CCD camera (ORCA-R2, Hamamatsu Photonics). For excitation, an Nd:YLF-laser (PL3143A-10, Ekspla) was used at a wavelength of 263 nm and a pulse duration of 10 ps, which is necessary to ensure a sufficient temporal resolution.

For every operating point, 1000 images were accumulated to increase the SNR. Afterwards, a background correction regarding the thermal noise of the camera was performed. It should be mentioned that a very small red-shift of the fluorescence emission spectrum would result at an excitation wavelength of 263 nm compared to 266 nm [41]. We do not expect that such small changes in the photon energy will have a significant impact on the fluorescence behavior. Suto et al. [53] presented only a very small deviation of the absorption cross-section of 1-MN at 266 nm from the absorption cross-section at 263 nm.
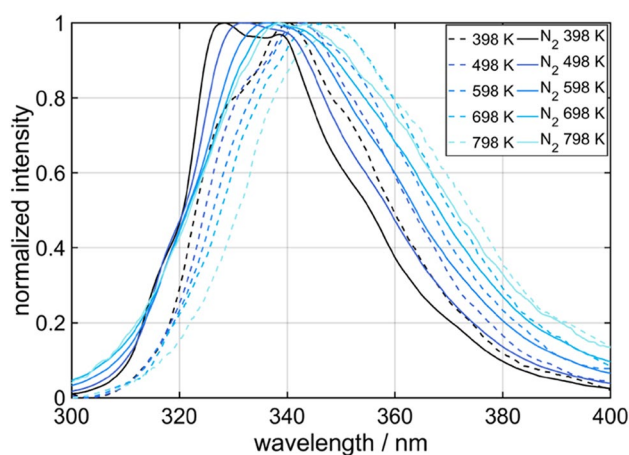
Fig. 4 Emission spectra of 1-MN PLIF at 1.0 MPa and temperatures from 398 to 798 K for $\Phi = 2$ (dashed line) and pure nitrogen [54] (solid line)

4 Results and discussion

First, in Sect. 4.1, the emission spectrum and decay times are analyzed for a general discussion of the influencing factors; the decay time is an important quantity to judge effects of different parameters on the fluorescence and de-excitation processes. Afterwards, the results are separated in Sects. 4.2 (FAR-LIF) and 4.3 (Two-color-detection).

4.1 Spectral and temporal fluorescence characterisation

Figure 4 shows a comparison of the emission spectra of 1-MN in dependency of the temperature at $\Phi = 2$ (dashed line) and in pure nitrogen [54] (solid line). Each spectrum is normalized to its maximum value.

The spectra in nitrogen and air/nitrogen mixtures are clearly shifted and broadened with increased temperature. This is due to the above-mentioned higher excess energy and the fluorescence emissions resulting from these highly exited vibrational states. In the presence of oxygen, the red-shift of the spectrum occurs as well and it is more distinct. In this case, besides the temperature-dependent intramolecular ISC, additional intermolecular ISC between the tracer molecule and the oxygen occurs. This leads to quenching of fluorescence, which is more probable for conditions at higher vibrational energy levels (i.e., at higher temperatures), and thus the red part of the spectrum is also affected by O_2 quenching at increased temperature. Thus, the difference in spectral shift of fluorescence between nitrogen- and oxygen-containing gas mixtures becomes smaller. This spectral red-shift increases with decreasing equivalence ratio (i.e., increased oxygen content, not shown here) and varies the slope of the fluorescence signal ratio for different equivalence ratios,
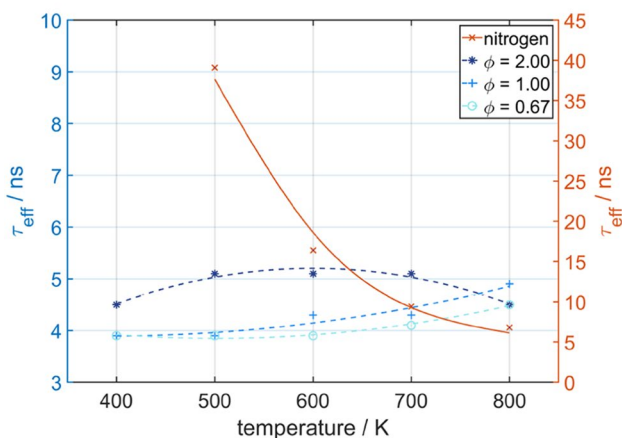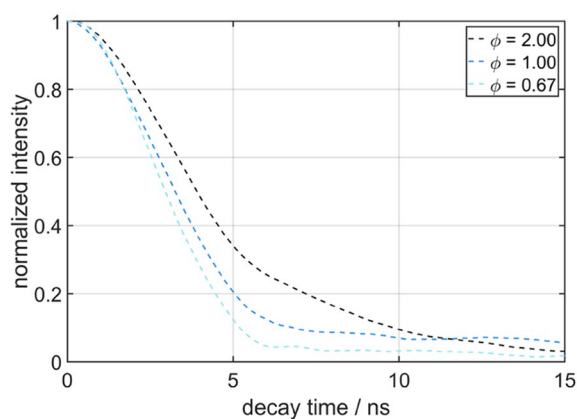

Fig. 5 Time-resolved fluorescence signal intensities of 1-MN at 1.0 MPa and various equivalence ratios at 600 K (top) and effective decay times τ at 1.0 MPa and various equivalence ratios (bottom). The effective decay times for nitrogen are added as well (these values extracted from Ref. [54]). Lines are inserted to guide the eye

which will be discussed in Sect. 4.3. This effect was also reported before by Kaiser and Long for naphthalene and 1-MN (at 0.1 MPa) [36] and it is also known for toluene [1].

Figure 5 shows the fluorescence decay time of 1-MN at 1.0 MPa. Examples of the time-resolved LIF intensities are shown for 598 K and 3 equivalence ratios $\Phi = 2$, $\Phi = 1$ and $\Phi = 0.66$ in Fig. 5 (top). The curves are extracted from accumulated data (1000 single measurements) normalized to their maximum values. It should be noted that temporal fluorescence trace initially deviates from a mono-exponential decay. A bi-exponential decay of 1-MN fluorescence (in CO_2 atmosphere) was already described by Benzler et al. [55]. In general, a non-exponential decay could be induced by collisional oxygen quenching [56]. In addition, the instrumental response function has to be taken into account [25], which was not the case in this work (however, the general trends of the lifetime depending on various parameters remain the same). For this purpose, further work has to be conducted to clarify this behavior.

Furthermore, in Fig. 5 (bottom) the effective decay times τ of 1-MN fluorescence for temperatures up to 798 K are extracted for these equivalence ratios and for nitrogen. The effective decay times were determined as the time where the fluorescence intensity had decreased to a fraction 1/e of the maximum signal intensity.

In nitrogen atmosphere, the decay time strongly decreases with increasing temperature due to the higher ISC probability [54]. This trend is in accordance to fluorescence decay times of naphthalene reported by Faust et al. [25] although the values of 1-MN are slightly smaller. In contrast, the decay time does not significantly change with temperature in the presence of oxygen for all presented equivalence ratios. The decay time of 1-MN is in the range of a few nanoseconds (less than 5 ns) for all three presented equivalence ratios and it is much shorter than in pure nitrogen atmosphere for all presented temperatures. This behavior can be explained by the strong oxygen-quenching effect in that range of equivalence ratios. At 600 K, the decay time at $\Phi = 0.67$ decreases by approximately 24% compared to $\Phi = 2$. The fluorescence decay time slightly decreases with decreasing equivalence ratio for temperatures from 400 to 700 K. This behavior confirms that oxygen quenching is the dominant process so that 1-MN should be an adequate tracer for FAR-LIF. In comparison to naphthalene [25], the 1-MN lifetime exhibits only weak pressure dependency. From 1 to 2 MPa, the fluorescence decay decreases by 20% for $\Phi = 2$ and by 5% for $\Phi = 0.67$ at 600 K (not shown here). The oxygen quenching of 1-MN is more distinct in comparison to toluene, which is also visible in the very high Stern–Volmer coefficient k_{SV} of 1-MN (which indicates the strength of fluorescence quenching; it depends on the quencher partial pressure instead of the number density). The Stern–Volmer coefficient is 1410 MPa^{-1} at 500 K for 1-MN [36] being much larger compared to ~ 300 MPa^{-1} for toluene at 500 K [57].

4.2 FAR-LIF

In this section, the FAR-LIF approach is studied in a wide range of parameter combinations. First, the signal dependency on the equivalence ratio is shown for various temperatures (Fig. 6). Later on, effects of pressure (Fig. 7) and fuel partial density (Fig. 8) are studied. For all measurements, the equivalence ratio was adjusted by variation of the amount of oxygen inside the bath gas (while the total amount of bath gas was kept constant by adding nitrogen). This ensures that the fluorescence signal intensity is measured for different fuel–air ratios without being additionally influenced by different fuel/tracer partial densities (which happens by changing Φ by a variation of the fuel partial density at a constant amount of oxygen). The error bar depicts the minimum and
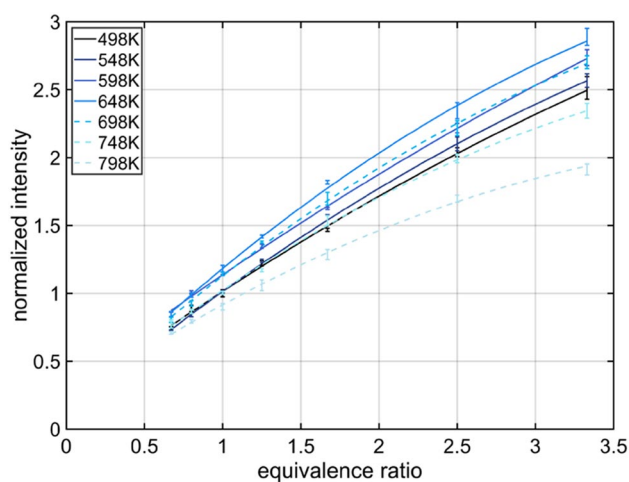

Fig. 6 LIF calibration for different equivalence ratios at temperatures from 498 to 798 K and pressure of 1.0 MPa. Fuel/tracer partial density is 12.6 g/m^3. Normalized mean values and the standard deviation (std) for the data are also provided in the supplementary material (Table S1). Lines are inserted to guide the eye
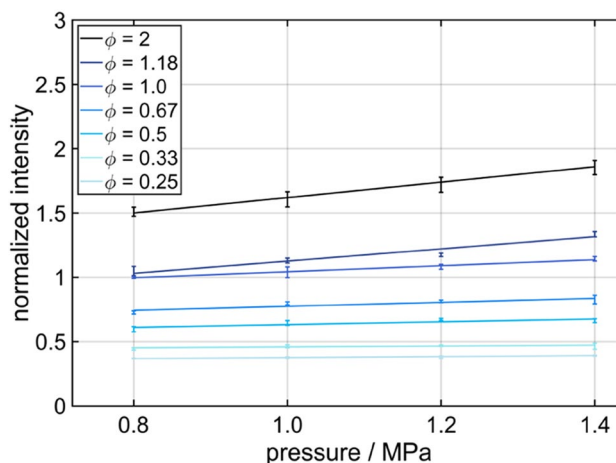

Fig. 7 1-MN LIF signal intensity as a function of pressure for different equivalence ratios from $\Phi = 0.25$ to $\Phi = 2$ at a temperature of 498 K. The fuel/tracer partial density is 6.7 g/m^3. Normalized mean values and the standard deviation (std) for the data are also provided in the supplementary material (Table S2). Lines are inserted to guide the eye

maximum value of three individual measurements (each consisting of 50 single images) for each operating point.

Figure 6 shows the fluorescence signal intensity as a function of the equivalence ratio Φ in a temperature range from 498 to 798 K. All signal intensities were normalized to 498 K and $\Phi = 1$. The pressure was set to 1.0 MPa and the partial density of the fuel/tracer mixture was set to 12.6 g/m^3 and kept constant during all measurements. The equivalence ratio was varied between $\Phi = 0.67$ and $\Phi = 3.33$.
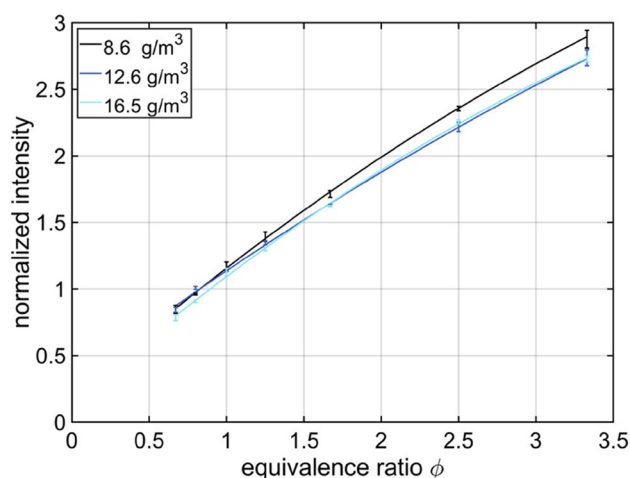
Fig. 8 LIF-calibration curve for different equivalence ratios at fuel partial densities of 8.6 g/m^3, 12.6 g/m^3 and 16.5 g/m^3 at a pressure of 1.0 MPa and a temperature of 598 K. Lines are inserted to guide the eye

The measurement shows an almost linear dependency of the signal intensity at least for equivalence ratios between $\Phi = 0.66$ and $\Phi = 1.66$. For higher equivalence ratios (i.e., lower oxygen concentrations), the slope decreases and the deviation from the FAR-LIF assumption increases (i.e., the function is not linear anymore). In this range of very fuel-rich mixtures, the fluorescence deactivation process is no longer entirely dominated by the quenching effect. An additional influence of the fuel partial density is discussed below.

For temperatures between 498 and 648 K, the slope and the offset of each calibration curve increase. This could be due to the broadening of the fluorescence spectrum with increasing temperatures [5] and the slightly increasing absorption cross-section [37]. For higher temperatures, the slope and offset decrease again. In this case, the decrease in total signal has a greater impact than the spectral broadening, and also the absorption cross-section decreases slightly for very high temperatures [5, 37]. This behavior could also be explained by a different temperature dependence of inter- and intramolecular ISC. With increased temperature, the probability of intermolecular ISC (quenching) is decreased (because of the lower O_2 number density with increasing temperature), while the intramolecular ISC is accelerated. The overlay of these two dependencies results in a temperature-dependent signal intensity without monotonous behavior, which is also known for toluene and naphthalene (in this case the fluorescence lifetime was investigated) [25]. This behavior was already described using a modified step-ladder model by Rossow [58]. In Fig. 5, we could not observe such distinct temperature effects in the fluorescence lifetime of 1-MN for varying FAR, this effect is just visible for $\Phi = 2$.

The temperature-dependent slope and offset of the FAR-LIF were also shown by Kaiser et al. [36] at ambient pressure conditions. In the data presented by Kaiser et al., a better linearity of the calibration curves (and thus a better match to the FAR-LIF assumption) is shown for moderate temperatures. However, as the equivalence ratio was adjusted by varying the fuel/tracer concentration, a real proportionality of signal intensity and equivalence ratio may not be given. Furthermore, at temperatures above 750 K, for naphthalene a so-called "third-decay channel" was reported [25]. Under these conditions, further non-radiative processes (potentially related to IC, which is similar to toluene) are enhanced. This would lead to lower fluorescence signals and shorter lifetimes. However, in Fig. 5, we could not verify this effect for 1-MN at 798 K in terms of reduced effective decay time.

Figure 7 shows the pressure dependency of the signal intensity at a constant equivalence ratio from 1.0 to 2.5 MPa. The equivalence ratio was varied in a wider range of $\Phi = 0.25$ to $\Phi = 2$. The temperature was set to 498 K. The fuel/tracer partial density was set to 6.7 g/m^3 and was kept constant during all measurements.

The signal intensity increases with increasing equivalence ratio for the entire pressure range because of the reduced oxygen concentration. For equivalence ratios from $\Phi = 0.25$ to $\Phi = 0.67$, no significant change of the signal intensity was found with increasing pressures. For larger equivalence ratios ($\Phi = 1$ to $\Phi = 2$), the signal intensity increases with increasing pressure. For $\Phi = 2$, the signal intensity increases by almost 25%. Due to relatively low amount of oxygen, the quenching effect is less pronounced and an increased impact of the vibrational relaxation is expected. Vibrational relaxation leads to higher fluorescence signal intensities while the probability of ISC and IC is reduced. The probability of vibrational relaxation usually rises with increasing pressures due to intermolecular collisions.

Figure 8 shows the fluorescence signal intensity as a function of the equivalence ratio Φ for different fuel partial densities of 8.6 g/m^3, 12.6 g/m^3 and 16.5 g/m^3. As mentioned above, a variation of the fuel and tracer partial density could also affect the FAR-LIF approach and needs special attention. Within every respective measurement, the fuel partial density was kept constant. The temperature was set to 598 K at a pressure of 1.0 MPa. The equivalence ratio was varied between $\Phi = 0.67$ and $\Phi = 3.33$. The measurements are normalized to 498 K, 1.0 MPa and $\Phi = 1$ (same as in Fig. 6).

As already described in Fig. 6, the signal intensity shows an almost linear behavior over the entire range of equivalence ratios. For 16.5 g/m^3 and 12.6 g/m^3, almost no difference in signal intensities exists. For 8.6 g/m^3, a small deviation is found to the signal at 16.5 g/m^3 with a maximum of about 9% at the largest equivalence ratio. At this ratio, the standard deviations (error bars) are also larger, and the deviation between the curves is similar to the combined
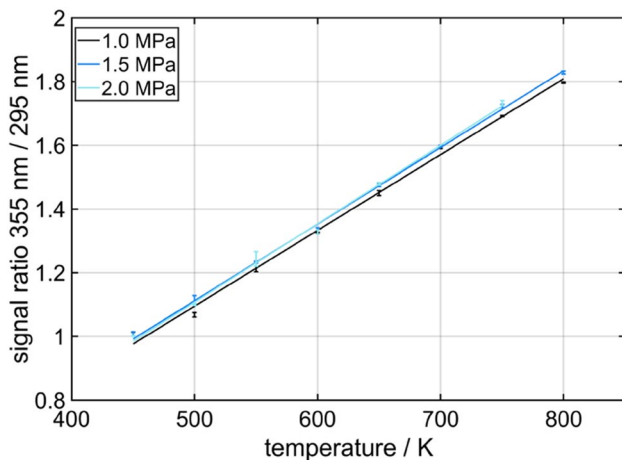
Fig. 9 Signal ratio 355 nm/295 nm of 1-MN PLIF over temperature at $\Phi = 1$ for pressures from 1.0 to 2.0 MPa. Lines are inserted to guide the eye

Fig. 11 Signal ratio 355 nm/295 nm of 1-MN PLIF over temperature at 1.0 MPa for nitrogen (dashed line) [5], $\Phi = 0.67$, $\Phi = 1$ and $\Phi = 2$. Normalized mean values and the standard deviation (std) for the data are also provided in the supplementary material (Table S3). Lines are inserted to guide the eye
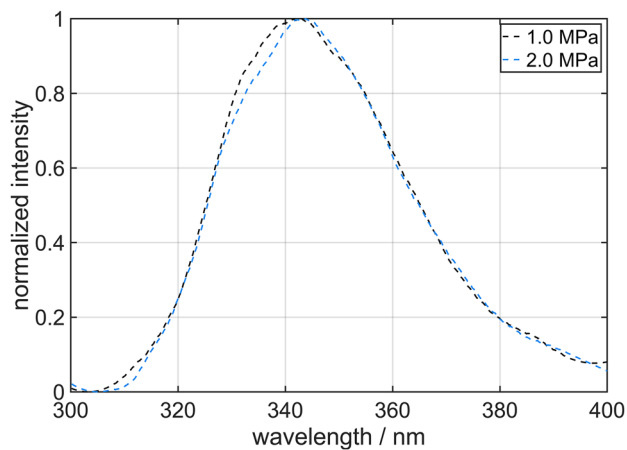

Fig. 10 Emission spectra of 1-MN PLIF at 500 K, $\Phi = 1$ and pressures of 1.0 MPa and 2.0 MPa

standard deviations. However, this is not true for smaller equivalence ratios. Further work should be performed to clarify this deviation.

4.3 Two-color-detection

In the following, the calibration regarding the two-color-detection is shown for varying pressure (Figs. 9, 10) and depending on the equivalence ratio (Fig. 11). For all measurements, the equivalence ratio was adjusted by variation of the amount of oxygen inside the bath gas (while the total amount of bath gas was kept constant).

Figure 9 shows the signal ratio 355 nm/295 nm as a function of temperature for pressures of 1.0 MPa, 1.5 MPa and 2.0 MPa at an equivalence ratio of $\Phi = 1$.
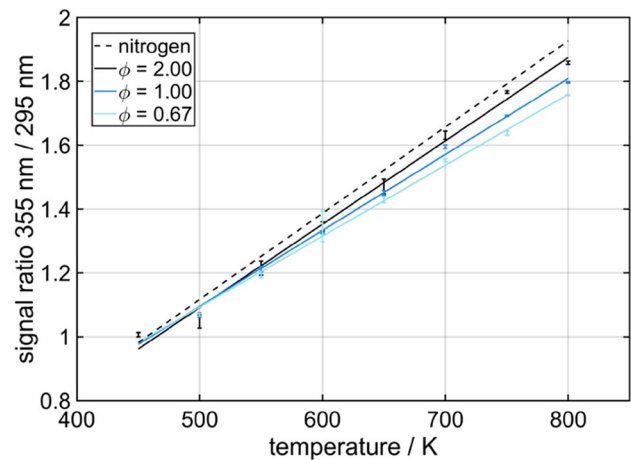
The measurements are normalized to their mean value at 450 K.

There is no significant pressure effect on the slope of the signal ratio and no appreciable effect on the shape of the emission spectra as reported above. Furthermore, no significant pressure effect on the position of the emission spectra is observed (see Fig. 10). The spectra shown are normalized to their maximum value. The same behavior was found for $\Phi = 2$ and $\Phi = 0.67$ (not shown here).

Pressure independency of the signal ratio in pure nitrogen atmosphere was already shown in the work of Lind et al. [5, 54] and Trost et al. [4]. Miles et al. [42] observed no significant pressure effects on the LIF signal of 1-MN in nitrogen up to about 5 MPa in an IC engine.

Finally, Fig. 11 comprises the two-color-calibration of 1-MN PLIF for nitrogen [5] and three equivalence ratios $\Phi = 0.67$, $\Phi = 1$ and $\Phi = 2$ at 1.0 MPa. The measurements are normalized to their mean value at 450 K.

For nitrogen, there is an increase of the signal ratio of about 20% per 100 K. With increasing equivalence ratio, this sensitivity decreases. The slope of the signal ratio decreases by ~8% for $\Phi = 1$ and by ~15% for $\Phi = 0.67$ relative to $\Phi = 2$. This effect has to be considered for temperature measurements in oxygen-containing environments. The effect of oxygen on the signal ratio was also shown for toluene [26]. In this case, the signal ratio in air decreases strongly in comparison to the signal ratio in nitrogen (excitation upon 248 nm). For 1-MN between 450 and 600 K, the deviations due to varied equivalence ratio are relatively small (less than 3% at 600 K between $\Phi = 2$ and $\Phi = 0.66$). This means that the same calibration curve could be used for all mixtures for thermometry and only a relatively small uncertainty would

result. However, especially for larger temperatures, an iterative solution is necessary for enabling a simultaneous determination of temperature and FAR at high accuracy.

5 Conclusion

In this work, the laser-induced fluorescence of 1-MN as function of equivalence ratio and temperature was studied in detail at elevated temperatures and pressures for the first time. Furthermore, the spectral emissions and fluorescence decay time in an oxygen-containing environment were investigated. Detailed calibration data were presented for a simultaneous determination of temperature via two-color LIF and equivalence ratio via FAR-LIF.

Regarding FAR-LIF calibration, an increase of the signal intensity was shown for increasing temperatures from 498 to 648 K. For larger temperatures up to 798 K, a decrease of the signal intensity occurs for the studied equivalence ratio range. In contrast, the fluorescence decay time did not show an appreciable temperature dependency for oxygen-containing mixtures. The temperature dependency of the signal may be explained by the temperature dependency of the absorption cross-section, which shows a similar trend. Probably, at very high temperatures, a "third decay channel" exists as another possible explanation for this temperature dependency, which was also reported for toluene and naphthalene [25]. In addition, also thermal decomposition and oxidation of the tracer and the base fuel may have an effect on the signal intensity at very high temperatures, which must be studied in future. No pressure dependency was found for lean equivalence ratios in the pressure range 1.0–2.5 MPa. At a pressure of 1.0 MPa and a temperature of 598 K, almost no influence of the fuel partial density was found.

For two-color LIF, a decreasing slope of the linear signal ratio 355 nm/295 nm and a spectral red-shift were observed for decreasing equivalence ratios (i.e., higher oxygen concentrations). This equivalence ratio-dependent slope must be considered for higher temperatures above 600 K to yield high-measurement accuracy. Again, no pressure influence on the signal ratio was found. In summary, this new set of calibration paves the way to simultaneous quantitative measurements of fuel distribution and temperature under realistic engine conditions.

References

1. C. Schulz, V. Sick, Prog. Energy Combust. Sci. **31**, 75 (2005)
2. M.C. Thurber, F. Grisch, R.K. Hanson, Opt. Lett. **22**, 251 (1997)
3. J.D. Koch, R.K. Hanson, Appl. Phys. B **76**, 319 (2003)
4. J. Trost, L. Zigan, A. Leipertz, D. Sahoo, P.C. Miles, Appl. Opt. **52**, 8001 (2013)
5. S. Lind, U. Retzer, S. Will, L. Zigan, Proc. Combust. Inst. **36**, 4497 (2017)
6. W. Koban, J.D. Koch, R.K. Hanson, C. Schulz, Phys. Chem. Chem. Phys. **6**, 2940 (2004)
7. S. Lind, S. Aßmann, L. Zigan, S. Will, Appl. Opt. **55**, 1551 (2016)
8. S.R. Engel, P. Koch, A. Braeuer, A. Leipertz, Appl. Opt. **48**, 6643 (2009)
9. A. Lozano, B. Yip, R.K. Hanson, Exp. Fluids **13**, 369 (1992)
10. S. Einecke, C. Schulz, V. Sick, Appl. Phys. B **71**, 717 (2000)
11. J. Trost, L. Zigan, A. Leipertz, Proc. Combust. Inst. **34**, 3645 (2013)
12. L. Zigan, J. Trost, A. Leipertz, Appl. Opt. **55**, 1453 (2016)
13. J. Reboux, D. Puechberty, F. Dionnet, SAE Tech. Pap. **94**, 1994 (1988)
14. W. Ipp, J. Egermann, I. Schmitz, V. Wagner, A. Leipertz, M. Hartmann, M. Schenk, SAE Tech. Pap. 2001-01-1977 (2001)
15. T. Blotevogel, M. Hartmann, H. Rottengruber, A. Leipertz, Appl. Opt. **47**, 6488 (2008)
16. P. Koch, M.G. Löffler, M. Wensing, A. Leipertz, Int. J. Engine Res. **11**, 455 (2010)
17. S. Lind, J. Trost, L. Zigan, A. Leipertz, S. Will, Proc. Combust. Inst. **35**, 3783 (2015)
18. T. Mederer, W. Friedrich, J. Trost, L. Zigan, M. Wensing, in *14. Int. Stuttgarter Symp.* (2014), p. 349
19. T. Mederer, M. Wensing, A. Leipertz, SAE Tech. Pap. 2013-01-0558 (2013)
20. W. Friedrich, R. Grzeszik, P. Lauschke, V. Zelenov, M. Wensing, SAE Tech. Pap. 2017-01-0779 (2017)
21. W. Friedrich, R. Grzeszik, M. Wensing, SAE Tech. Pap. 2015-24-2474 (2015)
22. W. Ipp, Analyse der Kraftstoffverteilung bei der Benzindirekteinspritzung (BDE) mit laseroptischen Meßverfahren. ESYTEC GmbH, Dissertation FAU Erlangen-Nürnberg, 2004
23. B. Peterson, D.L. Reuss, V. Sick, Combust. Flame **161**, 240 (2014)
24. J.D. Smith, V. Sick, Proc. Combust. Inst. **31**, 747 (2007)
25. S. Faust, G. Tea, T. Dreier, C. Schulz, Appl. Phys. B **110**, 81 (2013)
26. M. Luong, W. Koban, C. Schulz, J. Phys: Conf. Ser. **45**, 133 (2006)
27. W. Koban, J.D. Koch, R.K. Hanson, C. Schulz, Appl. Phys. B **80**, 777 (2005)
28. W. Koban, J.D. Koch, R.K. Hanson, C. Schulz, Appl. Phys. B **80**, 147 (2005)
29. S.A. Kaiser, M. Schild, C. Schulz, Proc. Combust. Inst. **34**, 2911 (2013)
30. B. Peterson, E. Baum, B. Böhm, V. Sick, A. Dreizler, Proc. Combust. Inst. **35**, 2923 (2015)
31. M. Luong, R. Zhang, C. Schulz, V. Sick, Appl. Phys. B **91**, 669 (2008)
32. B. Scott, C. Willman, B. Williams, P. Ewart, R. Stone, D. Richardson, SAE Int. J. Engines **10**, 2191 (2017)
33. P. Kranz, D. Fuhrmann, M. Goschütz, S. Kaiser, S. Bauke, K. Golibrzuch, H. Wackerbarth, P. Kawelke, J. Luciani, L. Beckmann, J. Zachow, M. Schuette, O. Thiele, T. Berg, SAE Tech. Pap. 2018-01-0633 (2018)
34. K.H. Tran, P. Guibert, C. Morin, J. Bonnety, S. Pounkin, G. Legros, Combust. Flame **162**, 3960 (2015)
35. Q. Wang, Y. Zhang, L. Jiang, D. Zhao, P. Guibert, S. Yang, Appl. Phys. B **123**, 242 (2017)
36. S.A. Kaiser, M.B. Long, Proc. Combust. Inst. **30**, 1555 (2005)
37. M. Orain, P. Baranger, B. Rossow, F. Grisch, Appl. Phys. B **102**, 163 (2011)

38. I. Berlman, *Handbook of Fluorescence Spectra of Aromatic Molecules* (Academic, New York, 1971)

39. B. Cheung, Tracer-based planar laser-induced fluorescence diagnostics: quantitative photophysics and time-resolved imaging. Stanford University, Dissertation Stanford, 2011

40. F. Payri, J.V. Pastor, J.M. Pastor, J.E. Juliá, Int. J. Engine Res. **7**, 77 (2006)

41. J.O. Uy, E.C. Lim, Chem. Phys. Lett. **7**, 306 (1970)

42. P.C. Miles, D. Sahoo, S. Busch, J. Trost, A. Leipertz, SAE Int. J. Engines **6**, 1888 (2013)

43. J. Trost, L. Zigan, A. Leipertz, D. Sahoo, P.C. Miles, Int. J. Engine Res. **15**, 741 (2014)

44. G. Tea, G. Bruneaux, J.T. Kashdan, C. Schulz, Proc. Combust. Inst. **33**, 783 (2011)

45. R.P.C. Zegers, M. Yu, C. Bekdemir, N.J. Dam, C.C.M. Luijten, L.P.H. de Goey, Appl. Phys. B **112**, 7 (2013)

46. D. Sahoo, B. Petersen, P. Miles, SAE Int. J. Engines **4**, 2312 (2011)

47. Bronkhorst, FLUIDAT on the Net, http://www.fluidat.com

48. ARAL, Safety Data Sheet for Diesel fuel according to DIN EN 590, https://www.aral.de/content/dam/aral/PDFs/Sicherheitsdatenbltter/Kraft_und_Brennstoffe/englisch/SGY2181_Aral%20Diesel_EN.pdf

49. Institut für Arbeitsschutz der Deutschen Gesetzlichen Unfallversicherung (IFA), GESTIS-Stoffdatenbank, http://www.dguv.de

50. I. Glassman, R.A. Yetter, N.G. Glumac, *Combustion* (Academic, Boston, 2014)

51. Verein Deutscher Ingenieure VDI-Gesellschaft Verfahrenstechnik und Chemieingenieurswesen (GVC), VDI-Heat Atlas, vol. 11 (Springer, Berlin, 2013)

52. A.H. Lefebvre, V.G. McDonell, *Atomization and Sprays* (CRC Press, Boca Raton, 2017)

53. M. Suto, X. Wang, J. Shan, L.C. Lee, J. Quant. Spectrosc. Radiat. Transf. **48**, 79 (1992)

54. S. Lind, Multi-Parameter-Untersuchung der Gemischbildung in Verbrennungsmotoren unter Einsatz der laserinduzierten Fluoreszenz. Shaker Verlag, Dissertation FAU Erlangen-Nürnberg, 2016

55. T. Benzler, S. Faust, T. Dreier, C. Schulz, Appl. Phys. B **121**, 549 (2015)

56. C. Albrecht, in *Principles of fluorescence spectroscopy* ed. by J.R. Lakowicz, Analytical and Bioanalytical Chemistry, 3rd edn (Springer, Baltimore, 2008)

57. S.M. Faust, Characterisation of organic fuel tracers for laser-based quantitative diagnostics of fuel concentration, temperature, and equivalence ratio in practical combustion processes. Universität Duisburg-Essen, Dissertation Duisburg-Essen, 2013

58. B. Rossow, Photophysical processes of organic fluorescent molecules and kerosene—application to combustion engines. Université Paris-Sud, Dissertation Paris, 2011